1. CLIMATE AND ENVIRONMENTAL MODELLING

1.1 Convective Timelag and a Model for Tropical Variabilities

Reliable models of atmospheric circulation are needed to generate long-range forecasts for advanced planning and decision support. This is particularly true for countries like India whose economy relies considerably on agriculture, and hence on amount and spatio-temporal distribution of rainfall. In the global climate scenario also, the tropical dynamics play a major role in setting the pattern of world-climate as considerable portion of the energy required to drive the global atmosphere comes from tropical region in the form of precipitational heating. This heating and associated dynamics in the tropics exhibit a wide range of both temporal and spatial variabilities. Understanding the mechanisms of these convection induced variabilities can provide the basis of developing a better simulation and prediction model.

In our earlier studies on tropical variabilities the concept of a convective timelag (CTL) was proposed and explored analytically. A numerical model of the tropical anomaly circulation incorporating non-linear convectively forced internal dynamics has been developed. The performance of this model is presented below.

Structure of tropical variabilities

Simulation of the observed monthly structure of tropical variabilities is considered. We have examined the quantity

$$\Delta\sigma_{\xi}\ (x,y,m) = \frac{\left|\ \sigma_{\xi_0}(x,y,m) - \sigma_{\xi}(x,y,m)\ \right|}{\sigma_{\xi_0}(x,y,m)}$$

where $\sigma_{\xi_0}\ (x,y,m)$ is the standard deviation of the observed field ξ for the month m (m=1,12 for January to December). The observed data set consisted of the anomaly fields for 12 months for 8 years (1979-1987). The corresponding simulated quantity, $\sigma_{\xi}\ (x,y,m)$ represents the standard deviation from sixteen one-year model simulations with initial conditions for winter and summer from respective years. Both the observed and the simulated fields were normalised to their respective maximum values. It was found that both CTL and the structure of evaporation wind feedback (EWF), arising from the structure of underlying sea surface temperature (SST), have profound effects on the structure of the variabilities.

Fig. 1.1 shows the longitude-latitude distribution of $\Delta\sigma_u$ for non-uniform strength of EWF, for a CTL of half hour. It was found that out of four values of CTL, the value of half an hour produced the best results in terms of simulating the structure of variabilities. As can be seen from this figure, the model can simulate a large part of the observed variabilities.

Mechanism of intraseasonal and interannual oscillations

A prominent feature of the tropical circulation is the existence of a number of oscillations at different temporal and spatial scales. In the intraseasonal scale the most prominent one is the 30-50 day eastward propagating oscillation, while in the interannual scale the most well documented oscillation is the ENSO related variabilities. Hence, one of the requirements

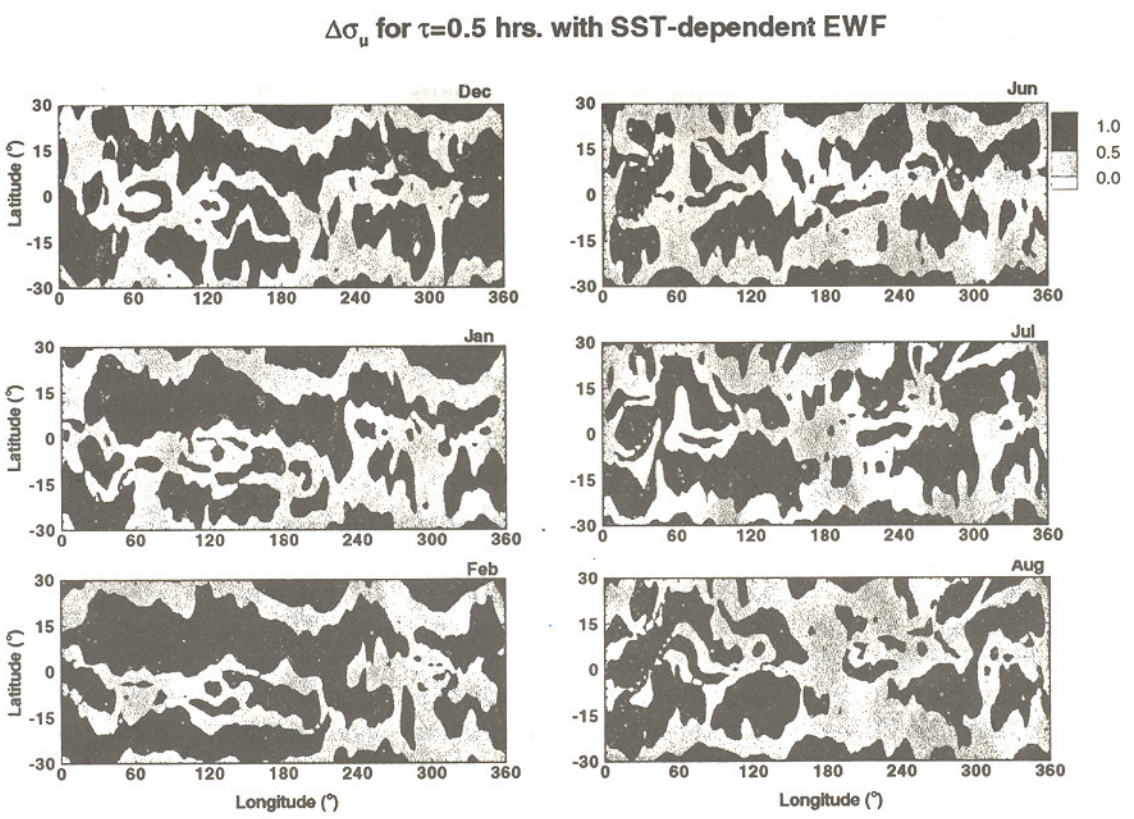

Fig.1.1: Longitude-latitude structure of the absolute value of $\Delta\sigma_u$ for winter (DJF) and summer (JJA) .

of a good tropical model is its ability to generate these variabilities. We have examined the existence and structure of oscillations at both intraseasonal and interannual timescales in our model. In the following, we discuss certain features of the simulated intraseasonal oscillations that show significant power above the red-noise level.

Fig. 1.2 shows the power spectra of a composite one-year model simulation filtered for 30-50 days centered at 40 days. The four curves in each panel represent the power spectra for four different values of CTL with a (SST induced) space-time dependent strength of EWF at different locations as indicated in the panels. As can be seen from these panels, the model in general supports ISO with 30-50 day time scale.

A more interesting result emerges in an analysis of the simulated time series around 10-20 days. As is well known, the monsoonal Indian ocean region exhibits a 10-20 days (or quasi-biweekly oscillation. This oscillation, characteristic of the summer monsoon region, significantly affects the monsoonal rainfall active and break conditions), and is not generally seen in other parts of the tropic. Figs. 1.3 and 1.4 present the results of power spectrum analysis for a 10-20 day window, centered at 15 days for the winter months (January-May) and the summer months (June-October), respectively.

A comparison of Figs. 1.3 and 1.4 also reveals that while in the summer months, the power is higher in the northern hemisphere, in the winter months it is higher in the southern hemisphere,

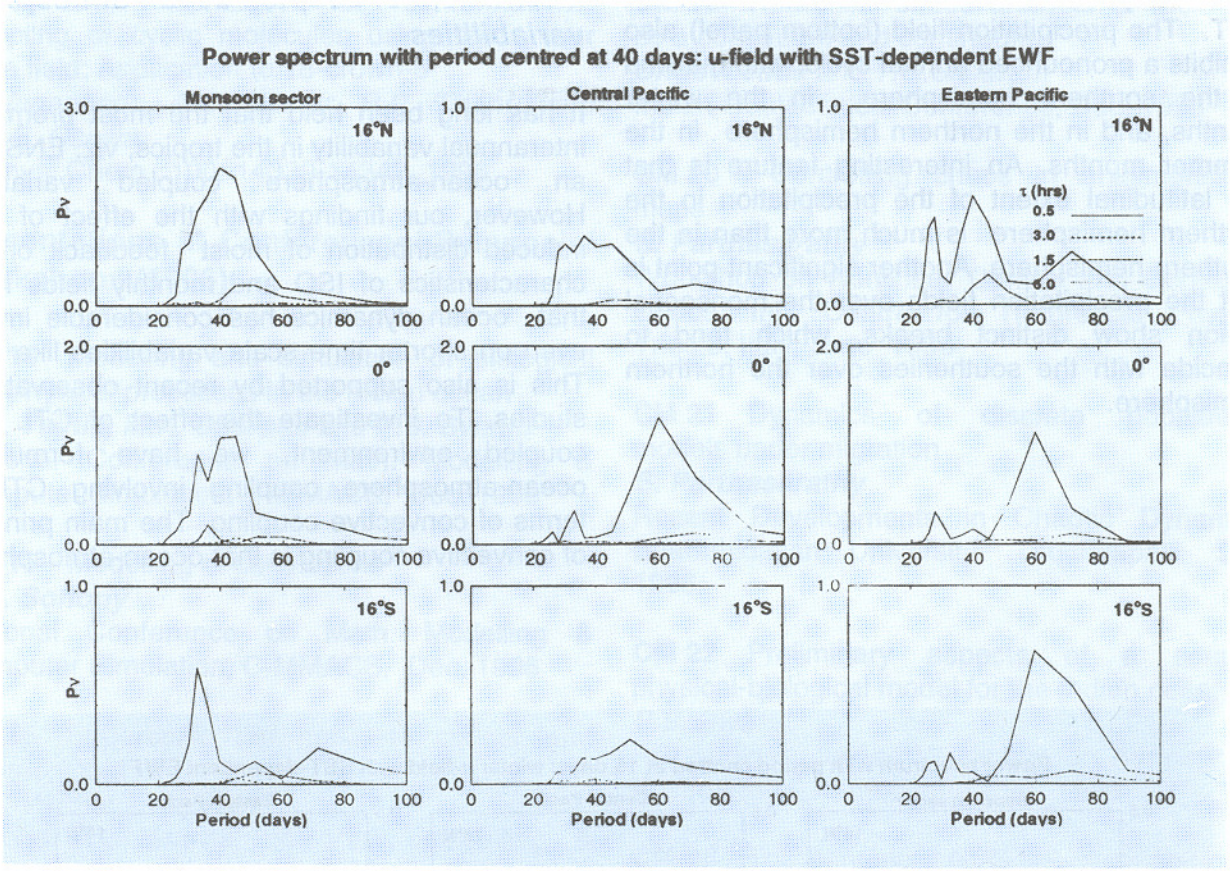

Fig.1.2: Power spectrum of the simulated filtered *u*-field centered at 40 days for different longitudinal and latitudinal positions.

as expected. This implies that the 10-20 day oscillation appears as a response of the anomaly circulation to the changing mean conditions over the summer monsoon region.

Annual cycle of tropical variabilities

We have examined sixteen one-year model simulations generated with initial conditions from observed anomaly fields for 1979 to 1987. The simulated fields for each integration are normalised to their respective maximum values. These are composited with equal weights to generate an ensemble average annual cycle of the model simulation. It is found that the model simulates a consistent annual cycle with distinct zonal characteristics.

Fig 1.5 shows the time-latitude structure of the composite simulated fields at 90° from 16 one-year model integrations. These sixteen integrations correspond to observed initial conditions for eight years (1979-1986), with two (winter and summer) initial conditions for each year. A scrutiny of the figure reveals several interesting features. For example, the anomaly westerly winds show a migration from the southern hemisphere to northern hemisphere as the season progresses. In particular, as in the case of mean winds over the summer monsoon region, the anomaly winds also show a transition from easterly (dashed contours) to westerlies. However, westerly during this period are also present over the southern hemisphere, unlike the mean component. The annual cycle in the meridional wind (second panel) over the monsoon region is marked by both northerlies and southerlies. The evaporation field (third panel) tends to follow the zonal wind, but not entirely. This is because of the fact that in our model the evaporation field is determined by both the anomaly wind and the SST field, through the

implicit dependence of the strength of EWF on SST. The precipitation field (bottom panel) also exhibits a pronounced annual cycle, with maxima in the southern hemisphere in the winter months, and in the northern hemisphere in the summer months. An interesting feature is that the latitudinal extent of the precipitation in the northern hemisphere is much more than in the southern hemisphere. Another significant point is that the precipitation fields over the monsoonal region show distinct breaks, which tend to coincide with the southerlies over the northern hemisphere.

Mechanism of coupled ocean-atmosphere variabilities

It has long been held that the most prominent interannual variability in the tropics, viz. ENSO, is an ocean-atmosphere coupled variability. However, our findings with the effect of SST induced distribution of moist feedback on the characteristics of ISO and monthly fields imply that ocean dynamics has considerable impact even on shorter time scale variabilities like ISO. This is also supported by recent observational studies. To investigate the effect of CTL in a coupled environment, we have formulated ocean-atmosphere coupling involving CTL in terms of convective coupling. The main principle of convective coupling is that ocean-atmosphere

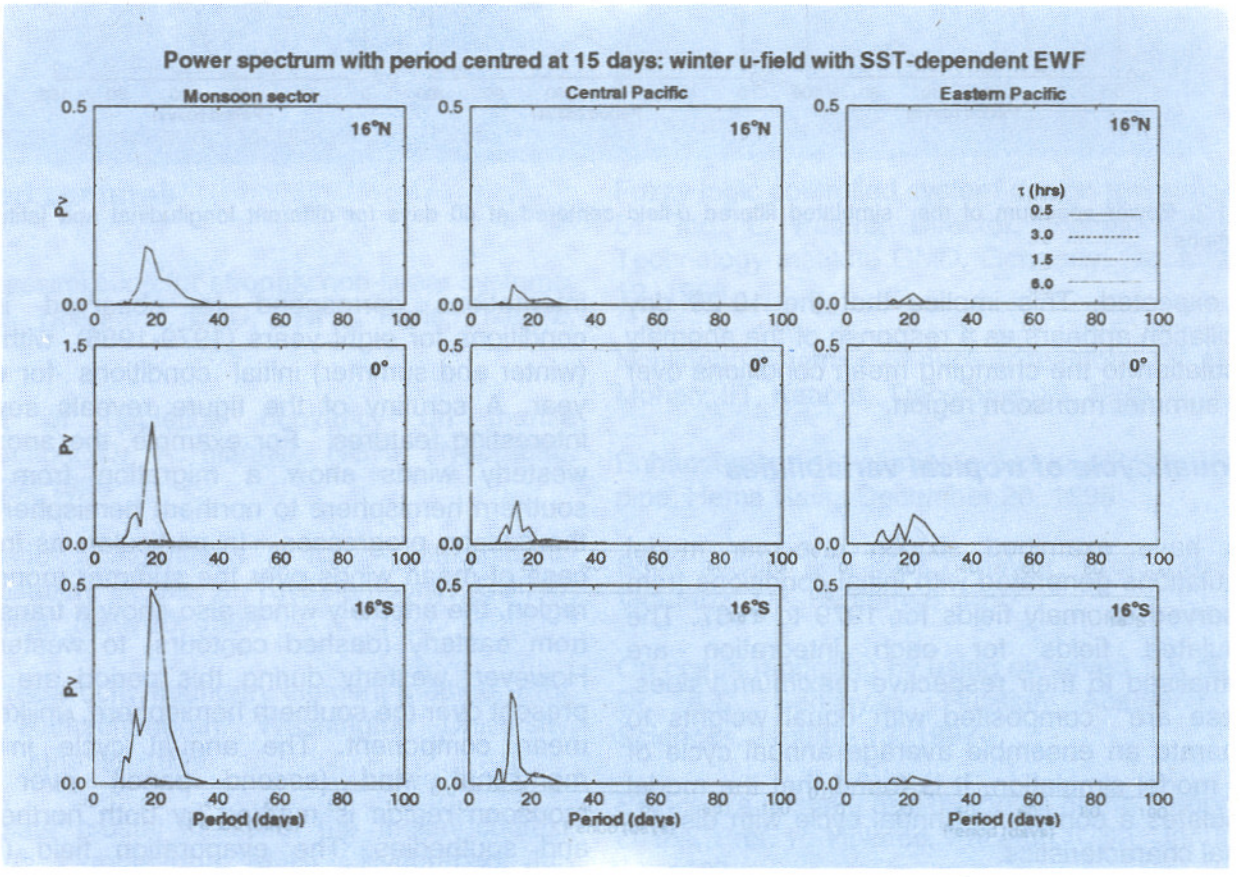

Fig.1.3: Power spectrum of the model simulated filtered *u*-field centered at 15 days for different longitudinal and latitudinal positions. Only winter months are considered.

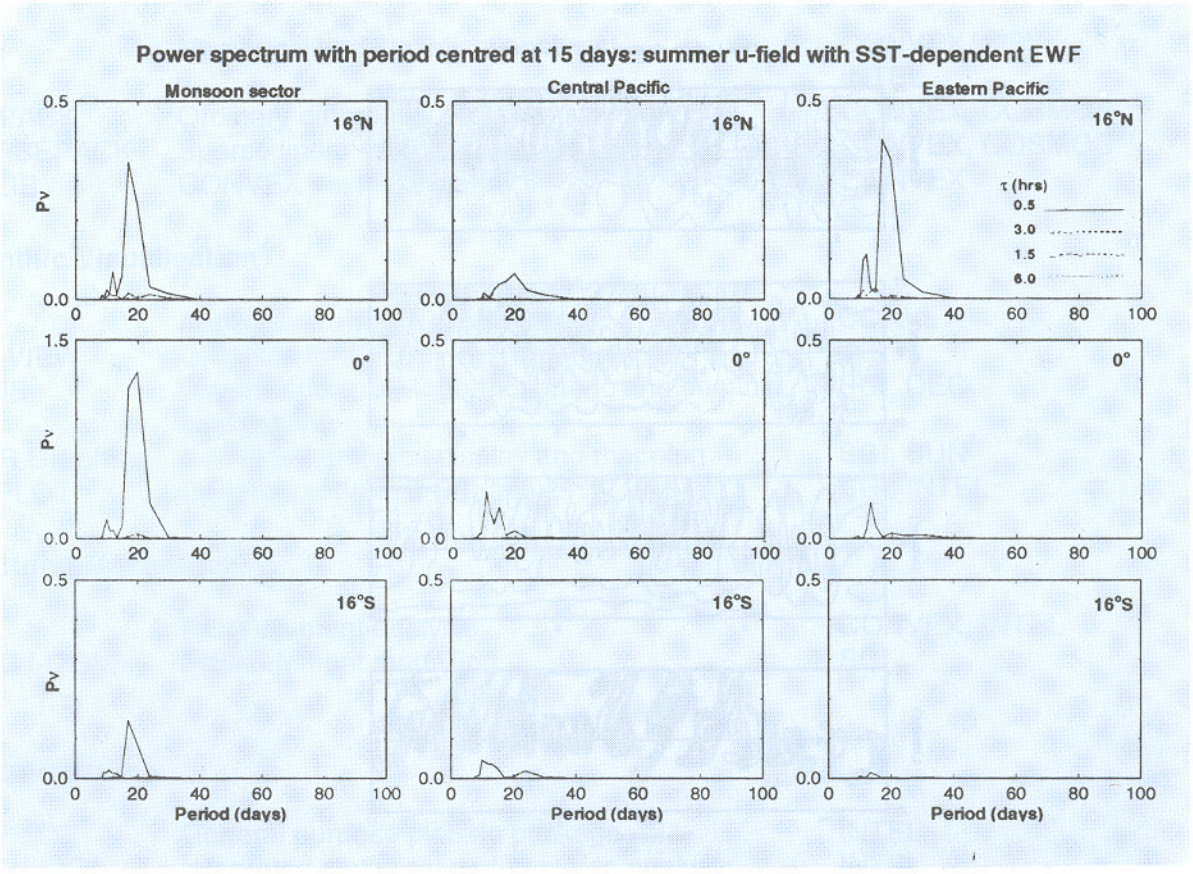

Fig.1.4: Power spectrum of the model simulated filtered *u*-field centered at 15 days for different longitudinal and latitudinal positions.Only summer months are considered.

Time Scales	Scenario Parameters				
	Δ (10^{-2})	G (10^{-1})	Γ	T (Days)	λ (10^{3} km)
Intraseasonal	5.0	6.5	1.4	89	26
	6.5	8.5	1.4	98	34
Seasonal	3.0	-21	1.5	206	33
	3.0	-12.5	1.3	202	15
Annual	3.0	-8.5	1.3	336	20
	2.5	-7.5	1.2	386	27
Interannual	2.5	-5.0	1.2	2310	23
	2.5	-7.5	1.2	1172	20

Table 1.1 Spectrum of convectively coupled oscillations

interaction, and in particular SST, can affect the atmospheric heating only by modulating atmospheric convection (or column precipitation).The atmosphere in the large scale is insensitive to underlying SST as a direct heat source. The implications of convective coupling are investigated for the dynamics of Kelvin waves.

Since the oscillations with widely different timescales take place over different mean conditions, two scenario - intraseasonal and interannual, are considered to take into account the effect of mean conditions. These two scenarios are characterised by certain model parameters that depend on the mean conditions. Table 1.1 shows the spectrum of convectively coupled oscillations for both intraseasonal and interannual scenarios. As can be seen from the table, convective coupling can give rise to a wide spectrum of variabilities at observed frequencies. *(P. Goswami, K. Rameshan*, * IIT, Kanpur)*

1.2 Sea Surface Height Simulations Compared with Satellite Altimeter Data

The Topex/Poseidon (T/P) altimeter is one of the most accurate satellite instruments available

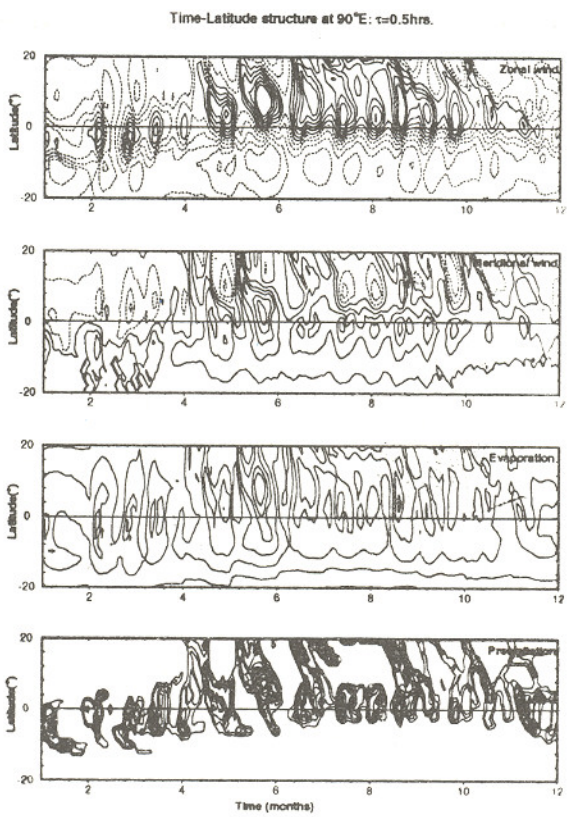

Fig.1.5 : Time-latitude structure of the simulated zonal wind, meridional wind, evaporation and precipitation fields from a composite of one-year simulation.

today. It measures the sea surface height (SSH) to an accuracy of 5-10 cm on a scale of a few hundred kilometres. The repeat cycle of the instrument is 10 days. We compare the SSH derived from Modular Ocean Model (MOM) simulations of Indian Ocean over a typical year with those of T/P to study the accuracy of MOM with a view to assimilating SSH form T/P into MOM at a later date when MOM is redesigned to compute SSH as a prognostic instead of a diagnostic.

The MOM run is global with a resolution of 1° in the longitude, $1/3^{\circ}$ in the latitude between 30^{0}S and 30^{0}N with coarser grids near the poles, and 20 levels in the vertical with 10 levels in the top 100 metres. There are a total of nearly 2 million grid points. The model is driven by monthly mean winds of Hellerman and Rosenstein and restoring conditions for temperature and salinity. The time step of the model is 45 minutes with surface boundary conditions interpolated to each time step based on values of the current and preceding or succeeding months. The mixing in the vertical is by the variable Philander-Pacanowski scheme which is based on the gradient Richardson number. Horizontal mixing is held constant in the entire domain. The SSH is computed from the depth-integrated streamfunction by solving an additional Poisson equation obtained by taking the divergence of the depth-integrated momentum equations at each time step. From the 15th year of MOM integration, we computed 10 day averages of SSH synchronised to the Julian days of T/P data from 1993.

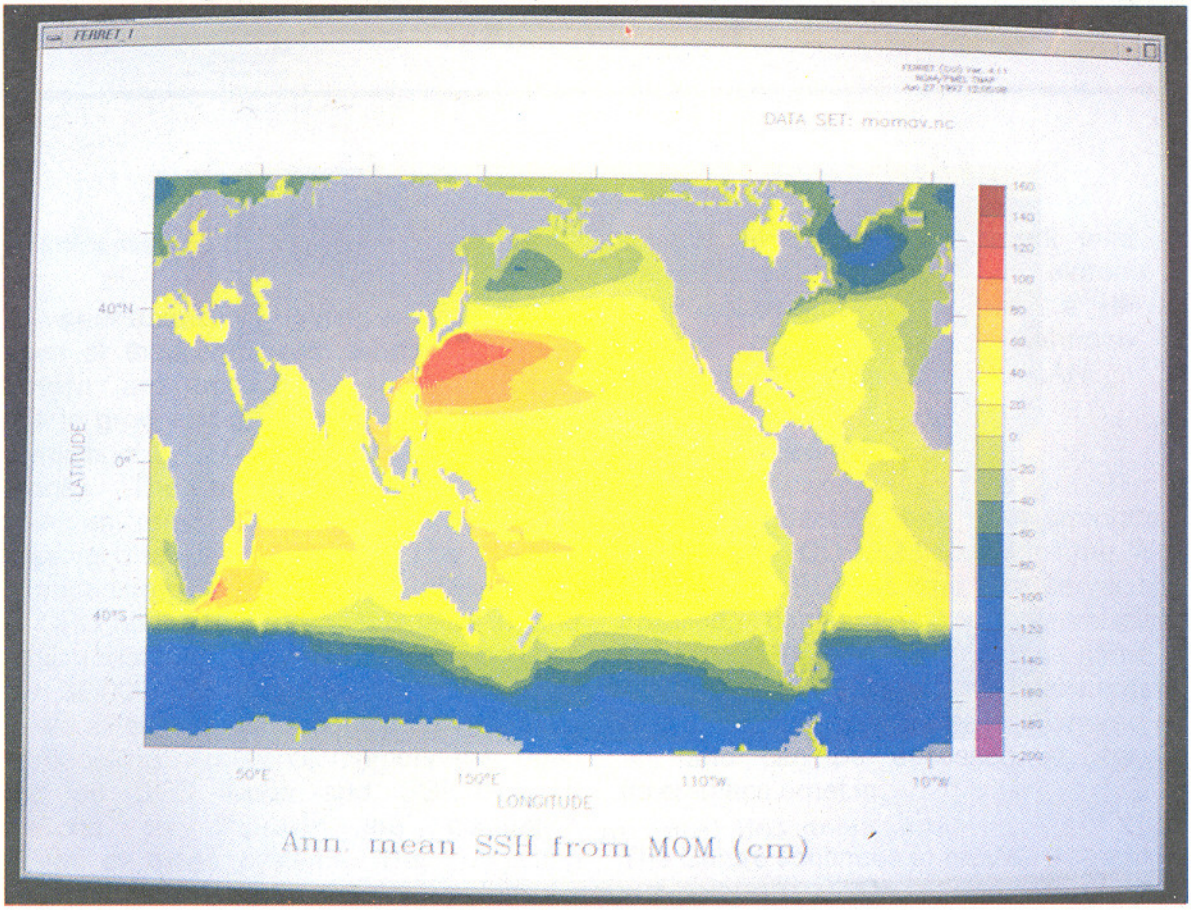

Fig. 1.6: Global annual-mean sea-surface height computed by the Modular Ocean Model.

Figs. 1.6 and 1.7 show the global annual-mean SSH computed by MOM and T/P respectively. Although the two are referred to slightly different datums, T/P to the local geoid and MOM to global zero-mean level, the agreement between the two is seen to be quite good.

We have compared the anamolies (differences from the annual mean) to offset the effect of different datums. Our intention is to show that both data sets have similar spectral behaviour at larger time scales of a month or more. Fig. 1.8 shows the coherence between the two data sets for a period of 66 days obtained from a cross-spectral density estimation procedure. A high coherence between the two data sets over most of the Arabian Sea and the northern Indian Ocean is seen. The phase relationship between the two is shown in Fig. 1.9 The two signals are seen to be in phase over regions of high coherence.

Efforts are underway at C-MMACS to redesign MOM so as to relax the rigid-lid condition and facilitate the computation of SSH as a prognostic variable. This would enable one to assimilate SSH data from satellites into MOM during integration. *(P.S.Swathi)*

1.3 Arabian Sea Ecosystem Modelling

The non-linear dynamical model for marine ecosystem earlier used to study the sensitivity of monthly averages to six model parameters and to estimatethe ranges of these parameter values by comparing with JGOFS cruise data in Arabian Sea.Detailed simulations are carried out at one

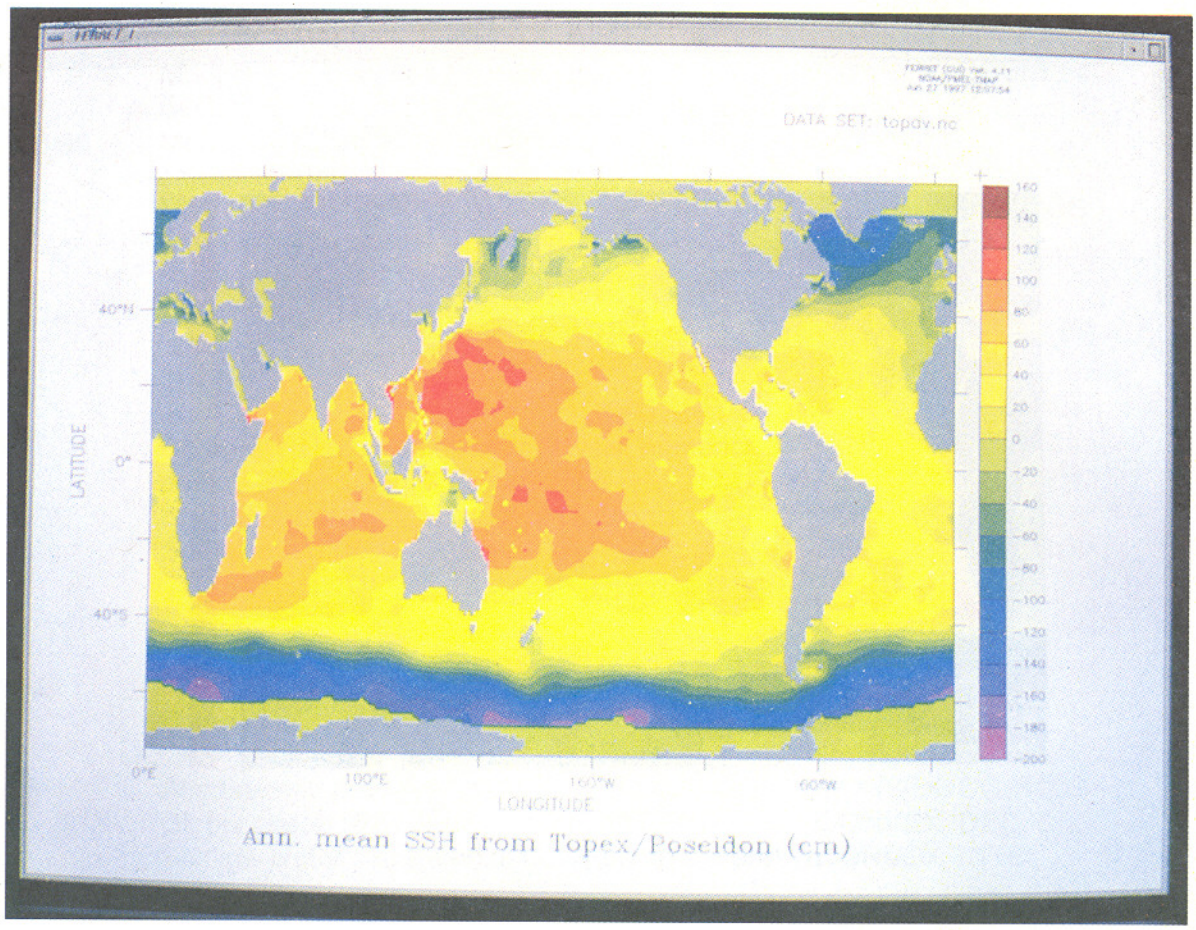

Fig. 1.7: Global annual-mean sea-surface from Topex/Poseidon data. Note the presence of small scale spatial variations in this figure and their absence in Fig. 1.6. The reason for this difference is the smoothed forcing in MOM. Also notice the presence of highs in the western pacific and the Indian ocean and the lows in the Antartic in both figures.

station (16^0N, 65^0E) to study the behaviour of the ecosystem for two versions of grazing by zooplankton, namely, non-switching (grazing preferences are independent of prey density) and switching (grazing preferences depend on prey density). It is noticed that marked preference of zooplankton for phytoplankton give unrealistic chlorophyll values for the non-switching version, whereas all the cases for switching version are within the acceptable range of chlorophyll. It is also observed that non-switching version gives rise to marked oscillations in chlorophyll values. Monthly averages of chlorophyll, zooplankton and bacteria (Fig. 1.10) show two significant peaks and a third small peak in winter, in the non-switching version, but the phytoplankton peaks are significantly broader. This is due to the large contribution of regenerated production in the total primary production in both the versions. The switching version flattens out these peaks markedly (Fig. 1.10). It is noted that in both the versions, zooplankton contributes a large fraction of the total biomass as the zooplankton grazes not only on phytoplankton but also on bacteria and on detritus. Since this type of relative abundance is not observed in temperate seas, it could be a distinguishing feature of the ecosystem in the tropical seas.

The zooplankton debris and sediment flux play a significant role in the export of nitrogen and

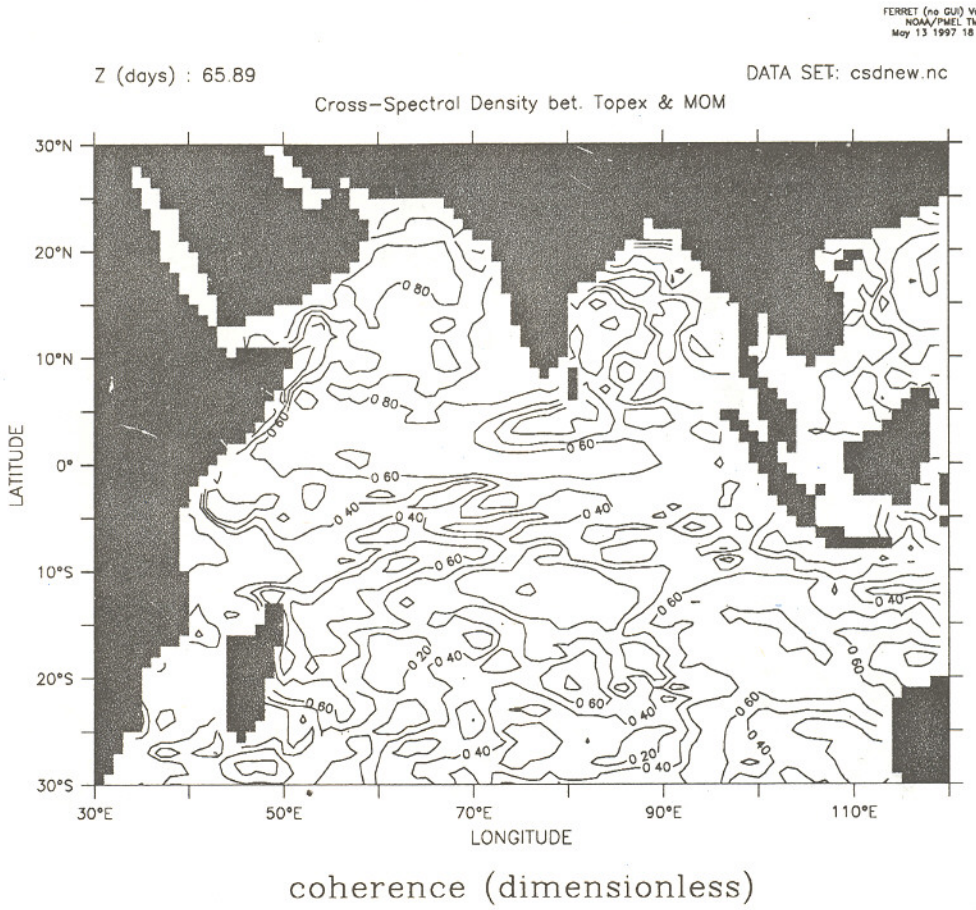

Fig.1.8 : Coherence between sea-surface heights of MOM and Topex/Poseidon for a period of 66days obtained from a cross-spectral density estimation procedure. Note the high coherence between the two data sets over most of the Arabian Sea and the northern Indian Ocean.

carbon to deep ocean. It is also noted from simulation results that primary production correlates well with chlorophyll and sediment flux (Fig. 1.11), thus providing a partial theoretical basis for using empirical correlations to estimate primary production from satellite measurements of chlorophyll and sediment trap measurements. It is also seen from the model results that the common assumption that there is equilibrium of total nitrogen in the mixed layer is onlyapproximately true. Some aspects of the model are being modified to capture the observations. *(M.K.Sharada)*

1.4 A Coupled Physical-Biological Model of Indian Ocean

The Arabian Sea, especially the waters off the Somali Coast, is perhaps the most active region of biological productivity in the world. The plentiful availability of nitrates which are upwelled during the South West Monsoon is one of the primary reasons for the high primary productivity. There is a distinct annual cycle in the productivity which can be seen from satellite photographs of ocean colour provided by the Coastal Zone Colour Scanner. A detailed zero-dimensional dynamical study of the marine ecosystem has

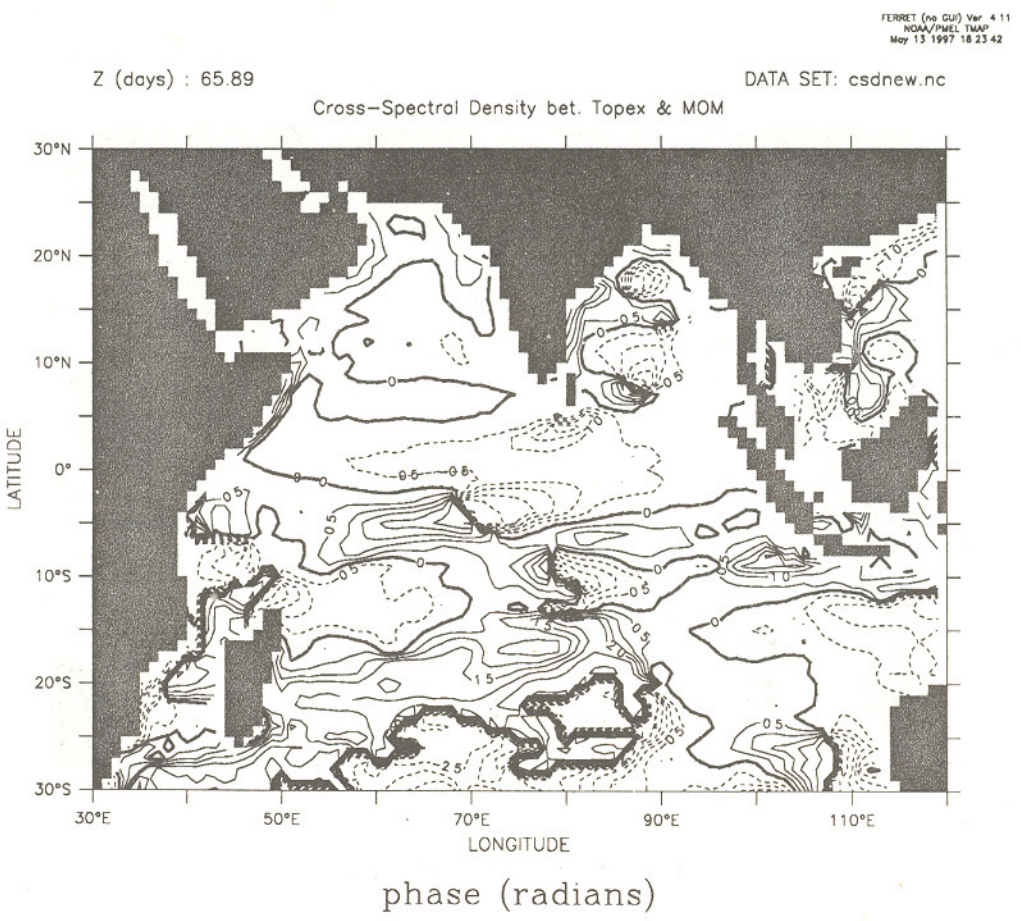

Fig. 1.9: Cross-phase between sea-surface heights of MOM and Topex/Poseidon for a period of 66 days obtained from a cross-spectral density estimation procedure. Note that the two signals are in phase over regions of high coherence (Fig. 1.8).

been performed (see Section 1.3). In this study we have coupled this model to include the effects of advection and diffusion. The biological model comprises of seven components; phytoplankton, zooplankton, bacteria and four forms of nitrogen, nitrates, nitrites, ammonium and detritus. The source minus sink terms of the tracer equations include terms which account for production, grazing and decay. Preferential grazing by zooplankton on phytoplankton, bacteria and detritus based on their availability is included. Below the euphotic zone, regeneration equations for conversion of dead organisms into nitrogen forms are employed.

The biological equations are coupled with MOM as additional tracers. However, these tracers are not conservative as vigorous interaction between the components takes place. The biological equations are integrated synchronously with flow equations. The model domain is 20^0S to 30^0N and 30^0E to 110^0E with a 1^0x1^0 resolution. Sponge boundary conditions were applied at the southern boundary to mitigate errors introduced at the boundaries. The resolution is too crude to permit a detailed analysis of the coastal fields but was considered enough for this preliminary study. In the vertical, the bathymetry of the sea bottom was introduced into the model along with

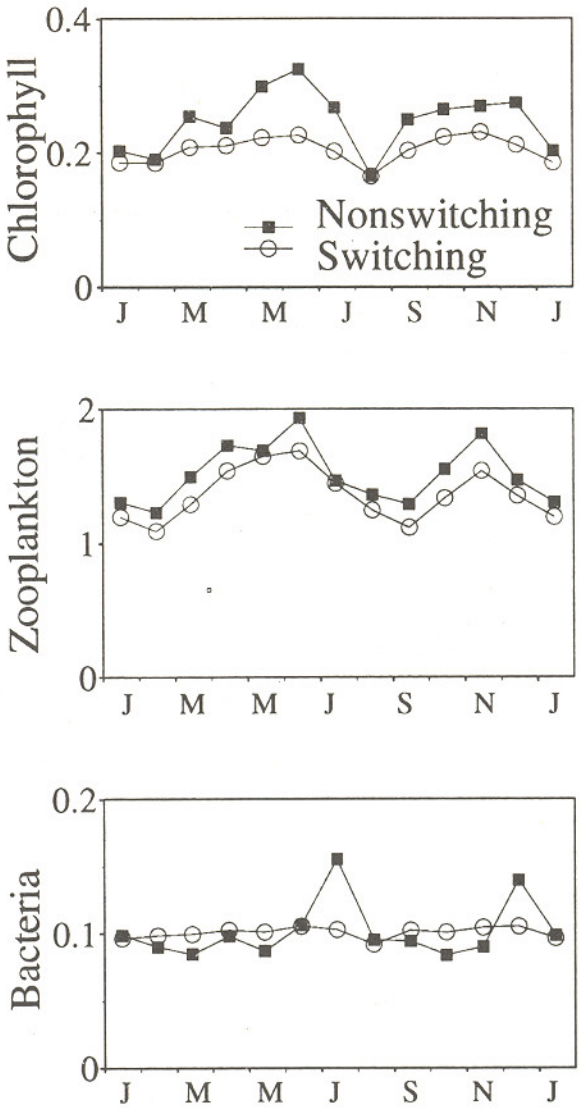

Fig 1.10: Monthly averages of chlorophyll (mg/cu m), Zooplankton and bacteria (m Mol N/cu m).

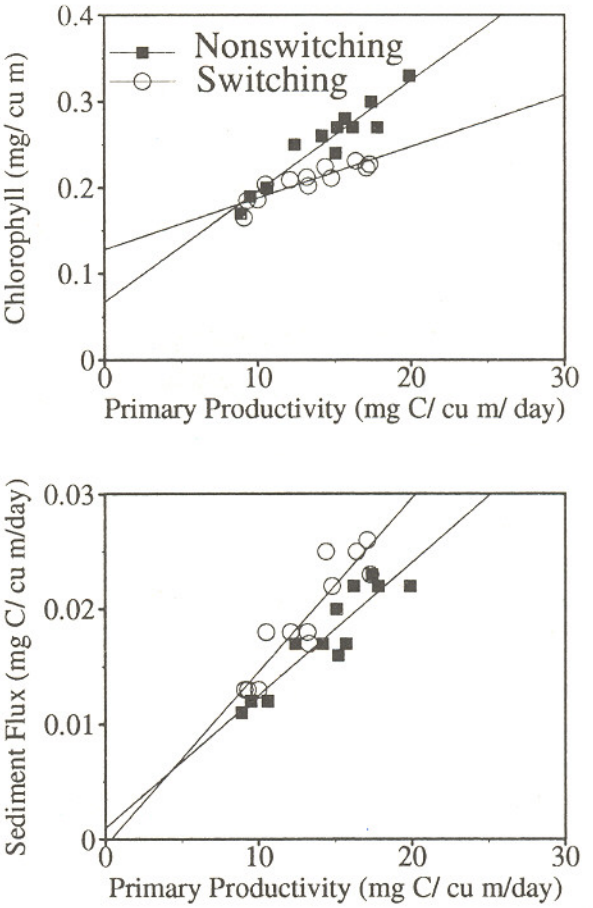

Fig. 1.11: Correlations between sediment flux and chlorophyll with primary productivity.

a vertical grid of 20 levels with 10 levels in thetop 100 metres. Solar radiation required to drive primary productivity is introduced from Oberhuber's Atlas of monthly mean values. Initial three-dimensional field of nitrate is introduced to the MOM grid from Levitus's 1994 Atlas. Other biological parameters were set to small non-zero initial values and allowed to evolve based on physical, growth, grazing and mortality laws.

The mixing scheme, vertical boundary conditions and the time step are identical to those employed in Section 1.2. The physical model is run for 20 years without biology for it to reach some kind of annual cycle. Biology is then introduced and the model is integrated for four more years. Snapshots of potential temperature, currents, nitrate, phytoplankton and zooplankton during the SW monsoon are shown in the front cover. Notice the strong currents of the Somali coast and the fall in temperature in that region due to intense upwelling. This is also evident from the panel for nitrate which shows an increase in that region.Also note the appearance of a bloom of phytoplankton near the Somali coast and the increased concentration of zooplankton slightly further away.

The time evolution of the biological field (not shown here) reveals the onset of the bloom in

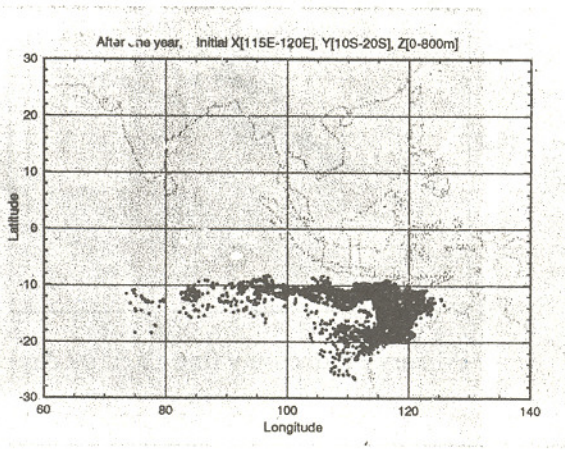

Fig. 1.12: Locations of the particles of the top layer (5 metres) at the end of one year. The particles were released on January 1 of the 16th year of MOM integration. See text for the locations of particle release. Note that only the northern and southern regions exhibit large scale spreading.

July, its persistence through September and its disappearance after that. The coupled model is now being run at fine resolution to capture the coastal features better. *(P.S.Swathi, M.K.Sharada)*

1.5 Lagrangian Particle Transport Study of the Indian Ocean Circulation

The warm pool of the Western Equatorial Pacific is believed to play a major role in the interannual climate variability such as ENSO. The Indonesian Throughflow (ITF) region is the primary pathway for the transport of heat and salt from the Pacific to the Indian Ocean. The Indonesian Archipelago is characterised by a strong complex seasonal variability in the upper ocean due to reversal of winds associated with the Asian and Austral monsoons. This leads to complex circulation patterns where fluid particle trajectories and streamlines are quite different. From a fluid dynamical view point, the implication of chaotic particle paths is that they lead to enhanced mixing.

In order to analyse the particle trajectories, we released 10,000 particles in the volume between 10^0S and 20^0S, 115^0E and 120^0E, and 0 to 800 meters, and followed them for a year. The system of first order differential equations for particle locations was solved synchronously with the MOM time step of 45 minutes. We have computed finite time Liapunov exponents, diffusion coefficients and correlation dimensions at each time step.

Fig. 1.12 shows the locations of the particles of the top layer (5 metres) at the end of one year. The particles are released on January 1 of the 16th year of MOM integration. We notice that only the northern and southern regions exhibit large scale spreading. The northern edge of the release volume is at the mouth of the Lombok Strait which accounts for the bulk of the ITF transport. There is very little transport to the east of the release volume. The westward transport is consistent with the transport expected by the South Equatorial Current which prevails throughout the year. There is very little meridional spreading as the sub-tropical gyre acts as a barrier to transport, akin to the "irrational tori" in classical models of chaotic advection. The vertical sections (not shown here) show that there is very little spreading at depth below 200 metres. In addition, stable stratification of the ocean acts effectively to prevent active mixing across depths. A detailed study of all aspects of chaotic mixing is currently in progress. *(B. Joseph, P.S.Swathi)*

1.6 Role of Low and High Clouds in Intensification of Tropical Cyclones

The crucial role played by the cloud processes in the dynamics of tropical cyclones is well known. Although the larger contribution to this cloud forcing comes from the high clouds, extending upto the tropopause, the lower level clouds also

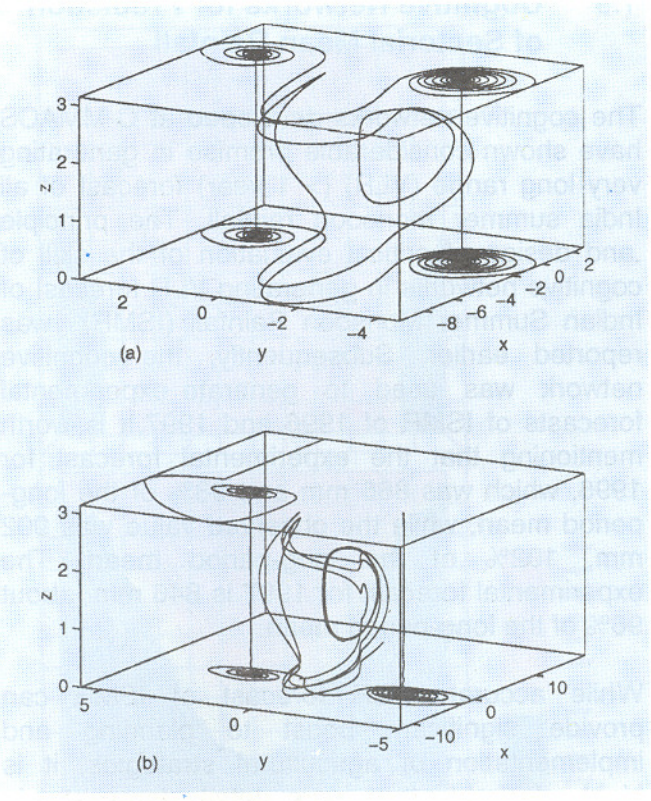

Fig 1.13: (a) Particle trajectories in an integrable monsoon flow (b) Particle trajectories in a 'chaotic' monsoon flow.

play important roles. The present study investigates and attempts to quantify the relative roles of low, medium and high clouds in the process of intensification of tropical cyclones. This question is being investigated in the context of a numerical model of tropical cyclones. viz. Wada's model. This model has been validated and used in several earlier studies and provides a realistic representation of the axisymmetric tropical cyclone dynamics. A series of numerical experiments are designed to evaluate the response of an incipient vortex to changes in the moist static energy, S of the clouds. The main parameter for measuring this response is taken as the percentage change in the maximum low-level tangential velocity, v_{max} for a given change in the cloud's moist static energy. To generate a reasonable sample, the numerical experiments were carried out by taking the Fig. 1.13 (a) Particle trajectories in an integrable monsoon flow (b) Particle trajectories in a 'chaotic' monsoonal flow mean thermodynamical state for several stations and different months. It was found, as expected, that a reduction (enhancement) in high clouds reduces (increases) the value of v_{max}. However, an interesting result is that, in contrast to high level clouds, an enhancement (reduction) in S for low or middle clouds leads to a reduction (enhancement) in the intensity. Thus a reduction in S for high cloud and a simultaneous enhancement in S for low or middle cloud appears to be the best combination for affecting a reduction in intensification of tropical cyclones. *(K Bhattacharya, P. Goswami)*

1.7 Chaotic Transport in a Simple Monsoonal Flow

It is a well-known fact that transport of moist maritime air masses from over the southern oceans is a major determinant of monsoon activity over the Indian subcontinent. For a detailed study one needs to consider the 'active' nature of moisture which may be considered as a tracer. In the present study we hypothesize that a better understanding of the 'passive' tracer advection problem will shed light on several important dynamical aspects of transport phenomena in the real atmosphere.

A simple model of the monsoon circulation is considered. Based on ideas from dynamical systems theory, we address several questions which are of prime significance from a practical viewpoint. Some of these issues are (a) Will Lagrangian chaos favour or weaken the monsoon activity? (b) How do equatorial intraseasonal waves intervene with the monsoon? (c) Which flow configuration leads to the active monsoon situation? In Fig. 1.13a, we present the Lagrangian picture of three particle trajectories in a simple monsoonal flow which is integrable (and therefore nonchaotic). Fig 1.13b shows that some of the trajectories exhibit signatures of chaos when the basic integrable flow is perturbed by an equatorial wave solution. *(B. Joseph)*

1.8 Analysis Of Tide Gauge Data for Sea Level Change

The linear methods used on the tide gauge data available for the stations in India depicting the sea level changes. Earlier the linear stochastic models were identified and the parameters were estimated for the given data. Further, the sea level variations for the stations in India, Singapore, Thailand and China show fractal nature indicating non-linearity present in the data. Therefore several non-linear models are used to describe the trend of sea level for certain stations. The non linear models considered are

Model I : $x(t) = ae^{bx(t-1)} + \varepsilon(t)$

Model II : $x(t) = \dfrac{ax(t-1)}{b + x(t-1)} + \varepsilon(t)$

Model III : $x(t) = ax(t-1)^b + \varepsilon(t)$

where *a* and *b* are the parameters; *x(t)* is the sea level at time *t* and *x(t-1)* is that at a lag of one year and $\varepsilon(t)$ is the random error. These models are used to analyse part of the data to estimate the parameters *a* and *b*. Using the estimated parameters the predictions for the known observed data are done for the stations shown in Table 1.2.

Stations	Observed	Predicted values through model		
		I	II	III
Bombay	2.5718	2.5473	2.5472	2.5472
Cochin	0.6750	0.6175	0.6950	0.6655
Madras	0.6494	0.6288	0.6264	0.5964
Vizag	0.8778	0.8214	0.8455	0.8217

Table 1.2: Observed and predicted sea levels

In all these cases some models perform better than the others. This work is being further extended for working out a general model for each coast/country. The data is also analysed using a technique in frequency domain called singular spectrum analysis (SSA). *(N.K. Indira)*

1.9 Cognitive Networks for Prediction of Sectorial Mean Rainfall

The cognitive networks developed at C-MMACS have shown considerable promise in generating very long range (VLR) (> 1 year) forecast of all India summer monsoon rainfall. The principle .and design of critical evaluation of the skill of cognitive networks in generating VLR forecast of Indian Summer Monsoon Rainfall (ISMR) was reported earlier. Subsequently, the cognitive network was used to generate experimental forecasts of ISMR of 1996 and 1997.It is worth mentioning that the experimental forecast for 1996, which was 866 mm and 98% of the long-period mean, while the observed value was 902 mm, 102% of the long-period mean. The experimental forecast for 1997 is 846 mm, about 96% of the long-period mean.

While accurate VLR forecast of ISMR can provide significant boost to planning and implementation of agricultural strategies, it is highly desirable that more detail forecasts, in terms of smaller coverage are generated. This, however is a formidable task, as the variabilities at smaller scales are much larger. This task is particularly difficult for conventional statistical models like power regression models since the observed parameters used for one scale (e.g. ISMR) are not readily applicable to another (say sectorial) scale.

A significant advantage of cognitive networks is that it does not require any other observed parameter other than past rainfall. The method is therefore readily applicable to other scales, in principle. The forecast skill of cognitive networks have been evaluated for one-year forecast of sectorial mean summer monsoon rainfall for three sectors, viz. Haryana, Punjab and Kutch .The results are shown in Fig 1.14 the top, middle and bottom panels in the figures represent Haryana, Punjab and Kutch, respectively. *(P. Goswami, P. Kumar)*

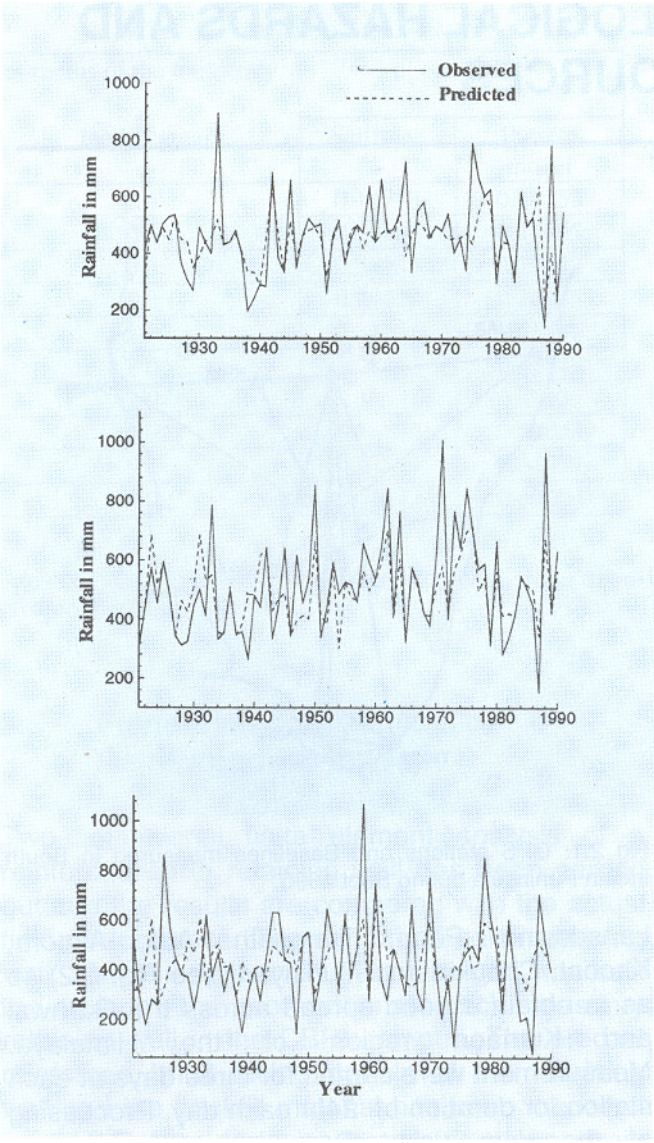

Fig. 1.14: Hindcast of the sectorial monsoon rainfall using cognitive network for 3 sectors.